Rotation in NGC 2264: a study based on CoRoT photometric observations

L. Affer, G. Micela, F. Favata, E. Flaccomio, J. Bouvier

Monthly Notices
of the
ROYAL ASTRONOMICAL SOCIETY

MNRAS **430,** 1433–1446 (2013) doi:10.1093/mnras/stt003

Rotation in NGC 2264: a study based on *CoRoT*⋆ photometric observations

L. Affer,[1†] G. Micela,[1] F. Favata,[2] E. Flaccomio[1] and J. Bouvier[3]

[1] *Istituto Nazionale di Astrofisica, Osservatorio Astronomico di Palermo G. s. Vaiana, Piazza del Parlamento 1, I-90134 Palermo, Italy*
[2] *European Space Agency, 8-10 rue Mario Nikis, F-75738 Paris Cedex 15, France*
[3] *UJF-Grenoble 1/CNRS-INSU, Institut de Planètologie et d'Astrophysique de Grenoble (IPAG) UMR 5274, F-38041 Grenoble, France*

Accepted 2013 January 2. Received 2012 December 20; in original form 2012 July 31

ABSTRACT

Rotation is one of the key stellar parameters which undergo substantial evolution during the stellar lifetime, in particular during the early stages. Stellar rotational periods can be determined on the basis of the periodic modulation of starlight produced by non-uniformities on the surface of the stars, due to manifestation of stellar activity. We present the results of an extensive search for rotational periods among NGC 2264 cluster members, based on photometric monitoring using the *COnvection ROtation and planetary Transits* (*CoRoT*) satellite, with particular attention to the distribution of classical and weak-line T-Tauri stars. NGC 2264 is one of the nearest and best studied star forming region in the solar neighbourhood, with an estimated age of 3 Myr, and is the object of a recent simultaneous multiband campaign including a new *CoRoT* observation with the aim to assess the physical origin of the observed variability. We find that the rotational distributions of classical and weak-line T-Tauri stars are different, suggesting a difference in the rotational properties of accreting and non-accreting stars.

Key words: stars: pre-main-sequence – stars: rotation.

1 INTRODUCTION

Over the last few years, the determination of stellar rotation rates for large samples of stars with different masses and ages in young open clusters, has made substantial progress, providing a large observational sampling of the angular momentum evolution of pre-main-sequence stars (Bouvier 2008, 2009). The precise mechanisms governing angular momentum evolution of pre-main-sequence low-mass stars are still not well understood, but basically they can be schematized with two main competing processes: star contraction and star–disc interaction. Stars in the pre-main-sequence phase are still contracting; thus, increasing their angular velocity to conserve the angular momentum. On the other hand, the observed existence of slow rotators and of a wide dispersion in rotation rates of cluster stars on the zero-age main sequence (ZAMS) can be explained only with the presence of a competing mechanism of angular momentum loss (i.e. spin-down of the star), different from star to star, during the pre-main-sequence phase. It is generally believed that this mechanism can be explained by the magnetic interaction between stellar magnetospheres and circumstellar discs, in a scenario known as *disc locking*, first proposed by Camenzind (1990) and Koenigl (1991) and explained in detail by Shu et al. (1994), which assumes that the angular momentum deposited on an accreting star (due to mass accretion from disc to star; Edwards et al. 1993) is exactly removed by torques carried along magnetic field lines connecting the star to the disc. The wide dispersion of rotational velocities observed on the ZAMS is the result of different disc lifetimes (Bouvier et al. 1993). Several observational results indicate a relation between the presence of discs and rotational evolution, in particular population of stars with discs, on average, rotate more slowly than those without discs and does exist a statistically significant anticorrelation between angular velocity and disc indicators such as near-infrared (NIR) excess and Hα equivalent width (EW; Bouvier et al. 1993; Edwards et al. 1993; Herbst et al. 2000, 2002; Lamm et al. 2005; Rebull et al. 2006). Moreover, the disc-locking scenario predicts that the torques arising from the magnetic connection between the star and the disc remove substantial angular momentum enforcing an equilibrium angular spin rate (Choi & Herbst 1996) which is in agreement with the constant rotation period in the 2–8 d range, characteristic of the majority of young stars. However, there have been several conflicting theoretical and observational evidences concerning the role of disc-locking scenario in the evolution of low-mass pre-main-sequence stars. Dahm & Simon (2005) pointed out that the $P_{\rm rot}$ distribution histograms for weak T-Tauri stars (WTTSs, whose periodic variability is believed to be induced by large starspots) and classical T-Tauri stars (CTTSs, whose variability may be also due to accretion spots and shadowing of the photosphere from dusty disc structures) in NGC 2264 are very similar and do not indicate that CTTSs are rotating more slowly than their WTTS counterparts.

⋆ The *CoRoT* space mission, launched on 2006 December 27, was developed and is operated by the CNES, with participation of the Science Programmes of ESA, ESA's RSSD, Austria, Belgium, Brazil, Germany and Spain.

† E-mail: affer@astropa.inaf.it

Furthermore, Dahm & Simon (2005) did not find a correlation between $P_{\rm rot}$ and theoretical age, as might be expected if stars were spinning up after decoupling from their discs. Stassun et al. (1999) and Cieza & Baliber (2006) did not find a correlation between accretion and rotation in Orion nebula cluster (ONC) and IC 348 low-mass stars, respectively (though they do not conclude that their results are inconsistent with disc locking). We have to note that most of the samples for which there is no clear evidence of a connection between the existence of discs and slow rotation, suffer from several biases, such as small sample size, sample biased towards small-mass or high-mass stars, the use of NIR photometry as disc indicator or the use of $v\sin i$ values instead of rotation periods, which make them unsuited to perform this kind of test, on star–disc interaction outcomes. In particular, the presence of a NIR excess does not guarantee that the star is actually accreting mass from a disc. The studies of Cieza & Baliber (2007) and Rebull et al. (2005), based on *Spitzer* mid-infrared (mIR) observations, however, as well as demonstrating that objects which currently show mIR excesses are more likely accreting than not, also found differences in the rotational properties of accreting and non-accreting stars for NGC 2264 and the ONC, respectively, and represent the best test case to date, providing the strongest evidence that star–disc interaction regulates the angular momentum evolution of pre-main-sequence stars.

The idea and the basic assumptions of disc locking, sketched above, are a simplification of a much more complex phenomenon, and indeed several discussions on the shortcomings of the theory and its confrontation with observations have been put forward. In particular, Matt et al. (2010, 2012) critically examined the theory of disc locking, noting that the differential rotation between the star and disc naturally leads to an opening (i.e. disconnecting) of the magnetic field between the two. They find that this significantly reduces the spin-down torque on the star by the disc, thus, disc locking cannot account (at least, alone) for the slow rotation observed in several systems and for which the model was originally developed. Matt et al. (2010, 2012) supported the idea that stellar winds may be important during the accretion phase, they may be powered by the accretion process itself and be the key driver of angular momentum loss (Hartmann & MacGregor 1982; Paatz & Camenzind 1996; Matt & Pudritz 2005). A strong magnetically driven wind, as proposed by Matt & Pudritz (2005), is an idea which deserves further study, as well as the development of a more realistic theoretical model able to explain the full range of observed rotation periods and magnetic phenomena and the achievement of a sufficient amount of accurate data to empirically constrain them.

NGC 2264 is one of the best known studied star forming regions in the solar vicinity ($d \approx 760$ pc, age $\approx$ 3 Myr) and is considered a benchmark for the study of star formation processes in our Galaxy. NGC 2264 luckily falls in the small portion of the sky accessible by *COnvection ROtation and planetary Transits* (*CoRoT*; Baglin et al. 2006), and thus represents a unique chance for the mission and the study of young stars still in a formation phase. Its distance and age make it an ideal *CoRoT* target, its size is well suited to the *CoRoT* field of view, with a large fraction of cluster members falling in the appropriate magnitude range for accurate photometric monitoring in the *CoRoT* observations.

NGC 2264 has been extensively observed at all wavelengths from radio to X-rays (see Dahm 2008 for a review on the region), for studies of the star formation process through the observation of its outcomes: the initial mass function (e.g. Sung et al. 2008), the star formation history and the spatial structure (e.g. Teixeira et al. 2006; Sung, Stauffer & Bessell 2009). NGC 2264 is also a primary target for the study of the evolution of the stellar angular momentum and its relation to circumstellar accretion (e.g. Lamm et al. 2005) of the evolution (and dispersal) of circumstellar discs (e.g. Alencar et al. 2010) and of the correlation between optical and X-ray variability of young stars (Flaccomio et al. 2010). Among several optical, infrared (IR) and X-ray surveys, both photometric and spectroscopic, on NGC 2264, the most recent are Sung et al. (2008), who have provided the widest area and deepest publically available optical photometry; Sung et al. (2009), who have published *Spitzer* (IRAC + MIPS) photometry; Rebull et al. (2002) and Dahm & Simon (2005), who have published spectral types, Hα and Li EWs, from low-dispersion spectra, for a total of $\sim$500 members; Fűrész et al. (2006), who have published radial velocities for 436 stars.

Lamm et al. (2004) performed a photometric monitoring of about 10 600 stars to search for periodic and irregular variable pre-main-sequence stars and found 543 periodic variables with periods between 0.2 and 15 d, and 484 irregular variables. Lamm et al. (2005) used this extensive study to conclude that the period distribution in NGC 2264 is similar to that of the ONC, though shifted towards shorter periods (confirming the conclusion of Soderblom et al. 1999, based on the analysis of the rotation rates of 35 candidate members, that the stars in NGC 2264 are spun-up with respect to members of the ONC).

The period distribution found by Lamm et al. (2005) is unimodal for masses lower than 0.25 $M_\odot$ while it is bimodal for more massive stars. Lamm et al. (2005) also found evidence for disc locking with a constant period, among 30 per cent of the higher mass stars (with a locking period of $\sim$8 d), while disc locking is less important among lower mass stars, whose peak in the period distribution at 2–3 d suggests that these stars have undergone a low rate of angular momentum loss from star–disc interaction, while not completely locked [an evolution scenario defined by Lamm et al. (2005) as 'moderate' angular momentum loss].

The bimodality is interpreted as an effect of disc–star interactions in pre-main-sequence stars, slow rotators being interpreted as stars that are magnetically locked to their discs, preventing them from spinning up with time and accounting for the broad period distribution of ZAMS stars. This assumption is supported by some observational results showing that WTTSs are rotating faster than CTTSs with inner discs (Bouvier et al. 1993; Edwards et al. 1993). Nevertheless, the hypothesis that accreting stars rotate more slowly than non-accreting ones is still a matter of debate, since conflicting evidence exists (see e.g. Stassun et al. 1999; Dahm & Simon 2005; Lamm et al. 2005; Rebull et al. 2005, 2006; Cieza & Baliber 2006, 2007), as explained above.

The *CoRoT* satellite has allowed us to conduct a large-scale survey of photometric variability of NGC 2264. Thanks to the accurate high-cadence photometry and large field of view of *CoRoT*, we could study rotation and activity of about 8000 stars in a 3.4 deg^2 region. The entire star-forming region fits into a single *CoRoT* field of view, and the campaign resulted in continuous 23 d LCs for 301 known cluster members brighter than $V \approx 16$ ($M = 0.3$–$0.4\,M_\odot$). The resulting optical broad-band LCs are the first accurate, highest cadence (32 or 512 s), longest duration, data set available for $\approx$3 Myr old stars.

So far, the *CoRoT* NGC 2264 data have been used to study the correlation between optical and X-ray variability in young stars (Flaccomio et al. 2010); asteroseismological properties of two high-mass cluster members (Zwintz et al. 2011); and to identify and study the behaviour of NGC 2264 members that are AA Tau like (Alencar et al. 2010).

Alencar et al. (2010) demonstrated that the peculiar photometric behaviour of AA Tau, which consist in a flat maximum in the LC interrupted by deep quasi-periodical minima (due to obscuring material with a variable structure which is located in the inner disc region, near the corotation radius), that vary in depth and width from one rotational cycle to the other, is quite common among CTTSs (Bouvier et al. 1999, 2003, 2007; Ménard et al. 2003; Grosso et al. 2007). The interpretation for AA Tau can now be considered quite solid, and its extension to a high fraction of CTTSs simply requires that the size of the obscuring clump of material (e.g. the height of the inner disc warp) is larger than previously thought.

In a rather similar scenario of circumstellar material orbiting the star and consequent time-variable shading, Flaccomio et al. (2010) found evidence of a correlation between soft X-ray and optical variability of CTTSs (no correlation is apparent in the hard band), while no correlation in either band (soft and hard) is present in WTTSs. Flaccomio et al. (2010) suggested that this observation is consistent with a scenario in which a significant fraction of the X-ray and optical emission from CTTSs is affected by temporally variable shading and obscuration.

The conclusions of both Alencar et al. (2010) and Flaccomio et al. (2010) point towards a different origin of the observed periods, suggesting a difference both in the physical and morphological properties of CTTSs and WTTSs.

In this paper, we derive accurate rotational periods of known NGC 2264 members, testing whether a relationship between accretion and rotation exists in pre-main-sequence stars.

In the following, we describe the observational and data reduction strategy (Sections 2 and 3). In Section 4, we discuss the results obtained and our major conclusions are summarized in Section 5.

2 *CoRoT* OBSERVATIONS

The first short run *CoRoT* observation (SRa01; P.I. F Favata) lasted from 2008 March 7 to 31 (23 d) and was devoted to the observation of the very young (∼3 Myr) stellar open cluster NGC 2264, which covers most of the mass sequence from ∼3 to ∼0.1 $M_{\odot}$.

A total of 8150 stars were observed, with right ascension (RA) between 99.°4 and 100.°9 and declination (Dec.) between 7.°6 and 10.°3 and *R* magnitudes from 9.2 to 16.0. The sample includes 301 cluster members (see Section 3 for details regarding membership criteria). We used the so called N2 data delivered by the *CoRoT* pipeline (Samadi et al. 2007) after correction of the electronic offset, gain, electromagnetic interference and outliers. The pipeline includes background subtraction and partial jitter correction. Low-quality data points, e.g. taken during the South Atlantic Anomaly crossing or due to hot pixels events, are flagged. Some of the stars have LCs in three separate but ill-defined bands (red, green and blue). In these cases, our analysis was conducted on the white-light data obtained by summing the three bands. The LCs are sampled at a rate of 512 s or oversampled at 32 s. All the LCs presented here were rebinned to 512 s. Using *CoRoT* photometry we are able to reveal luminosity variation, with a precision down to 0.1 mmag h^{-1} (magnitude between 11 and 16), during continuous observations, allowing us to measure photometric periods also in relatively quiet stars (for comparison, the luminosity variations of the Sun range between ∼0.3 and 0.07 mmag at maximum and minimum activity, respectively; Aigrain & Irwin 2004).

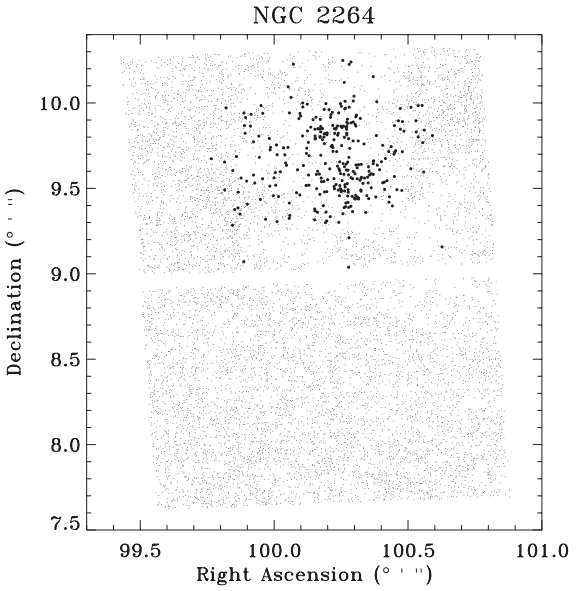

Figure 1. Spatial distribution of the *CoRoT* targets in the SRa01 (dots) with target stars satisfying one or more membership criteria (big dots), as described in the text.

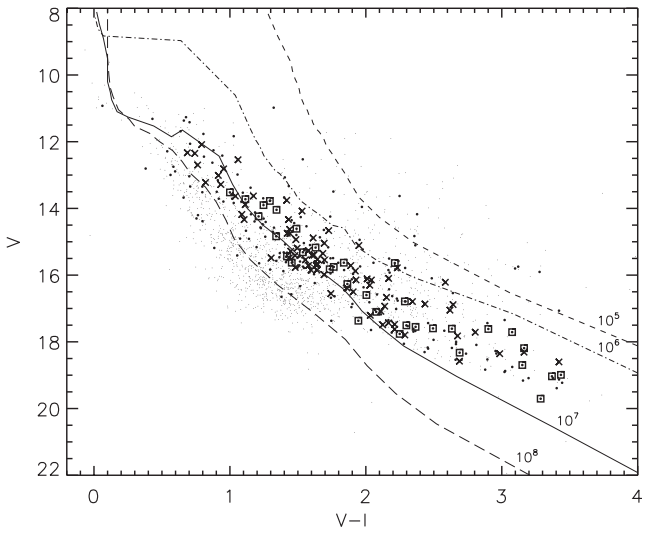

Figure 2. The colour–magnitude diagram of the 8150 SRa01 stars observed by *CoRoT* (grey dots). The large black dots indicate the 301 cluster stars satisfying one or more of the membership criteria. The crosses are WTTSs and the squares are CTTSs, defined following our criterium (WTTSs for $EW_{H\alpha} \leq 5$ Å and CTTSs for $EW_{H\alpha} \geq 10$ Å). The curves denote isochrones (yr) from Siess, Forestini & Dougados (1997) (transformed to the observational plane using the Kenyon & Hartmann 1995 compilation).

3 SAMPLE EXTRACTION AND LIGHT-CURVE ANALYSIS

We selected 301 cluster stars (whose spatial distribution is shown in Fig. 1 as big dots) satisfying one or more of the following membership criteria (the number of objects which fulfill the various criteria is indicated near each criterium).

(i) Detection in X-rays by *Chandra* ACIS or *XMM–Newton* (Ramírez et al. 2004; Flaccomio, Micela & Sciortino 2006; Dahm et al. 2007; Flaccomio et al., in preparation) and location on the

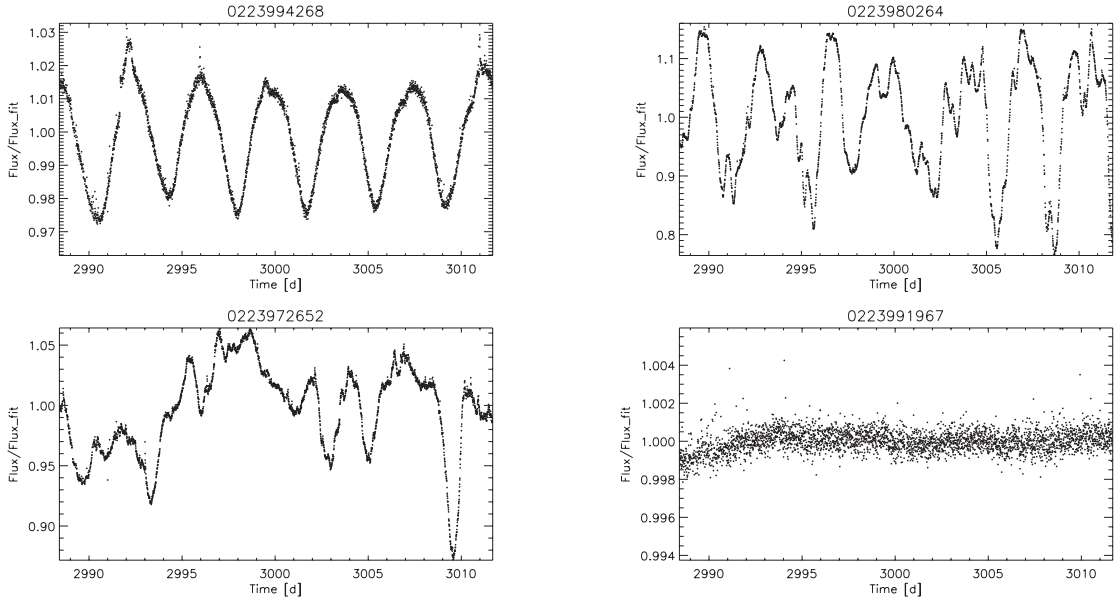

Figure 3. Four examples of morphologically different LCs (rebinned to 512 s): spot-like periodic (top-left panel); AA Tau-like system (top-right panel); irregular (bottom-left panel) and non-variable 'noisy-like' (bottom-right panel). Time is in days from 2000 January 01 (JD-245 1544.5).

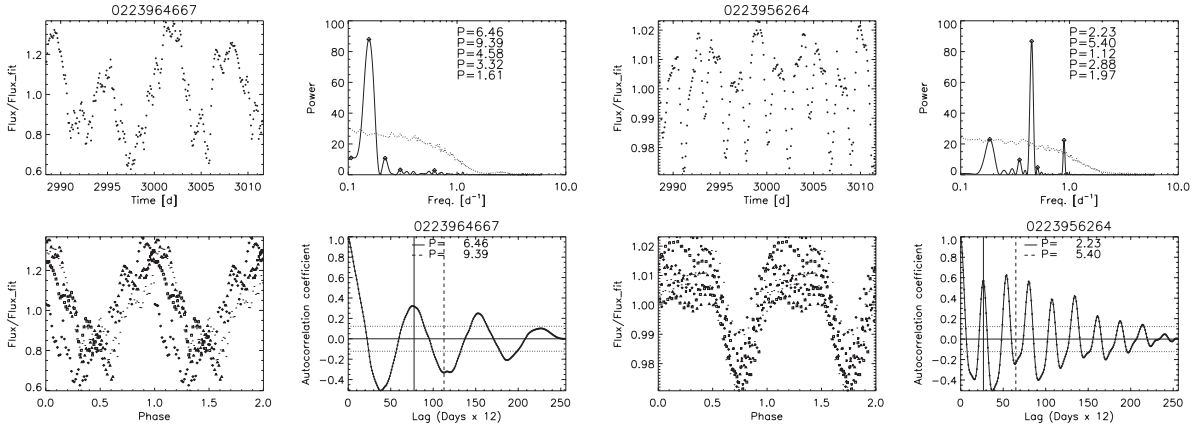

Figure 4. Two examples of NGC 2264 members: the four left-hand plots are for a CTTS, *CoRoT* ID 0223964667, while the four right-hand plots are for a weak line T-Tauri star, *CoRoT* ID 0223956264. For each example, the top panels show the LC and the relative LNP, with the dotted curve superimposed indicating the 1 per cent significance threshold determined by simulations (the periods indicated in the top-right of the LNP plot are the five most significant periods yielded by the Lomb-Scargle periodogram), while the bottom panels show the LC folded with the most significant period for each example, and the autocorrelation plot with the 95 per cent confidence interval (dotted horizontal lines) with the vertical lines indicating the position of the two most significant periods found with the LNP. Time in the LCs is in days from 2000 January 01 (JD-245 1544.5).

cluster sequence in the (I, $R-I$) diagram, when I and R magnitudes are available (191).

(ii) High levels of Hα emission, indicative of accretion, according to photometric indices (Lamm et al. 2004; Sung et al. 2008) (104).

(iii) Hα with spectroscopic EW greater than 10 Å and/or indicated to be in strong emission by Fűrész et al. (2006) (86).

(iv) Classified as Class I or Class II according to Sung et al. (2009), based on *Spitzer* mIR photometry (76).

(v) Strong optical variability + high Hα emission, indicative of high chromospheric activity, according to Lamm et al. (2004) (87).

(vi) Radial velocity members according to Fűrész et al. (2006) (192).

After selecting the cluster members, we classified them as CTTSs if their Hα EW was greater than 10 Å, and WTTSs if smaller than 5 Å. The threshold between these two classes is a function of spectral type, as suggested by Martín (1998) and deeply analysed by Barrado y Navascués & Martín (2003). The information regarding the Hα EW is available from the work of Dahm & Simon (2005) for 164 members, 86 with $EW_{H\alpha} \leq 5$ Å, 19 with $EW_{H\alpha}$ between 5 and 10 Å, and 59 with $EW_{H\alpha} \geq 10$ Å. We decided to exclude intermediate EWs ($5 < EW_{H\alpha} < 10$ Å), though not a usual procedure when dealing with Hα, to keep the two samples of CTTSs and WTTSs well separate and thus avoid possible ambiguity in the classification. In Fig. 2, we show the V versus ($V-I$) colour–magnitude diagram for the 8150 stars in the SRa01 observations with isochrones from Siess et al. (1997) (transformed to the observational plane using the Kenyon & Hartmann 1995 compilation), together with the NGC 2264 members.

We have analysed the *CoRoT* LCs as in Affer et al. (2012), we refer the reader to this work for a full description of data

Table 1. Samples used according to membership criteria, Hα EWs available from Dahm & Simon (2005) and membership-IR classification (Class II and Class III) following Sung et al. (2009).

Samples	Spot-like	AA Tau like	Irregular	Non-periodic	CII	CIII
301 members	189	20	45	47	42	114
164/301 (with Hα)						
59 CTTS (EW $\geq$ 10 Å)	23	12	23	1	22	6
19 intermediate (5 < EW < 10 Å)	12	1	5	1	7	2
86 WTTS (EW $\leq$ 5 Å)	77	2	6	1	4	59

Table 2. Catalogue of periods for NGC 2264 members.

CoRoT ID	Period (d)[a]	*AmpVar* (per cent)[b]	R	$B-V$	RA (J2000.0)	Dec. (J2000.0)	Memb-IR[c]	EW (Hα)[d]	Mass[e]
0223948127	I	20.7	15.000	−0.200	99.76562	9.67337			
0223951807	–	0.9	14.700	1.500	99.81503	9.65377			
0223951822	–	0.5	13.800	0.690	99.81532	9.49160			
0223952236	–	4.6	14.100	−1.020	99.82101	9.97097			
0223953966	3.987	3.7	12.600	−0.590	99.84448	9.28458			
0223954040	9.684	2.7	14.000	0.030	99.84557	9.60481			1.30
0223954556	–	0.7	13.800	0.400	99.85257	9.37606			
0223955032	5.436	5.3	14.300	0.460	99.85937	9.68647		−1.100	0.60
0223955438	–	0.7	13.400	2.200	99.86499	9.38587			
0223955517	–	0.2	12.900	0.520	99.86609	9.47768			
0223955994	–	0.7	13.300	0.040	99.87251	9.34971			
0223956264	2.229	6.5	14.800	0.470	99.87656	9.56053			0.80
0223956963	9.786 AA	15.6	14.700	−0.200	99.88675	9.07066			
0223957004	–	2.8	14.200	0.700	99.88737	9.94127			
0223957142	2.568	16.9	15.200	0.600	99.88912	9.86726			0.40
0223957322	18.05	8.1	15.300	0.850	99.89156	9.82254			0.80
0223957455	10.16 AA	28.0	15.200	0.500	99.89333	9.91437			
0223957734	–	8.1	15.300	0.690	99.89726	9.54231			
0223957908	–	0.7	13.600	0.810	99.89991	9.40729			
0223958794	–	2.7	14.200	0.730	99.91180	9.86451			1.60
0223958963	0.859	9.0	15.200	0.720	99.91379	9.93336			0.60
0223959618	3.922 AA	55.9	14.200	0.860	99.92274	9.77229			
0223959652	3.732	5.7	12.700	−0.170	99.92316	9.57808		−3.300	1.40
0223959949	–	0.6	14.800	0.770	99.92764	9.53115			
0223960995	–	0.6	14.500	1.310	99.94267	9.80571			
0223961132	3.839	9.3	12.500	0.210	99.94466	9.68178	III		1.40
0223961409	1.104	0.7	11.900	−0.030	99.94879	9.43535	III		
0223961560	–	1.4	12.700	1.570	99.95090	9.98496			
0223961941	6.52	4.3	14.700	0.400	99.95667	9.55630	III		1.10
0223962024	–	0.7	14.500	2.900	99.95769	9.93945			
0223962712	–	1.6	14.500	0.970	99.96801	9.31938			
0223963678	0.676	5.0	14.700	0.600	99.98199	9.79233	III		
0223963815	–	1.5	13.200	0.100	99.98402	9.51299			
0223963881	12.92	0.7	13.700	−0.400	99.98499	9.72557	III		
0223963994	–	0.2	15.200	−1.200	99.98674	9.74040			
0223964667	6.456	79.3	15.300	−0.200	99.99690	9.45691			
0223964830	2.575	9.1	15.900	0.530	99.99934	9.56164	III		0.80
0223965280	–	0.7	14.500	0.970	100.00603	9.51846			
0223965459	1.351	15.4	15.600	0.700	100.00892	9.75401	III		
0223965593	9.830	0.8	13.400	−0.100	100.01107	9.30565	III		
0223965989	0.819	7.3	15.300	0.760	100.01676	9.45211	III		0.60
0223967301	0.957	12.6	15.800	1.360	100.03550	9.73719	III	3.500	0.50

Table 2 – *continued*

CoRoT ID	Period (d)[a]	*AmpVar* (per cent)[b]	*R*	*B* − *V*	RA (J2000.0)	Dec. (J2000.0)	Memb-IR[c]	EW (Hα)[d]	Mass[e]
0223967602	1.236	7.0	13.300	0.470	100.04005	9.69555	III	−1.700	1.50
0223967803	3.841	7.7	14.300	0.600	100.04288	9.64872	III	2.000	0.70
0223968039	I	56.9	15.900	0.400	100.04640	9.63503		52.90	0.90
0223968398	2.702	11.0	15.800	1.130	100.05183	9.73986	III	3.600	0.50
0223968439	8.688	31.6	15.400	−0.200	100.05240	10.09474	II		
0223968646	–	2.0	15.400	0.500	100.05598	9.32465			
0223968688	1.117	3.9	11.500	0.080	100.05666	9.41396	III		2.20
0223968804	1.295	3.9	13.600	0.660	100.05841	9.34141	III		1.40
0223969098	I	158.2	15.800	1.300	100.06316	10.03289			
0223969672	–	7.2	16.000	1.000	100.07179	10.22651			
0223970440	–	3.7	14.700	0.260	100.08372	9.47472		3.200	
0223970694	1.467	5.2	13.000	0.010	100.08755	9.60907	III	0.300	1.50
0223971008	7.38	9.9	15.900	1.800	100.09258	9.90811	III	2.100	0.60
0223971231	I	170.8	14.500	−0.340	100.09618	9.46190		49.50	1.10
0223971383	4.648	11.9	15.800	0.550	100.09904	9.92345	II	80.60	
0223971866	7.015	2.7	12.600	0.360	100.10703	9.97667	III		
0223971984	6.281	14.0	15.500	1.480	100.10938	9.63385	III	3.500	0.60
0223972652	I	21.4	13.000	−0.900	100.11988	9.51704		39.10	
0223972652	–	21.4	13.000	−0.900	100.11988	9.51704		1.800	1.60
0223972691	7.206	12.0	15.300	1.310	100.12061	9.70490	III	1.700	0.90
0223972918	–	0.9	14.100	0.930	100.12383	9.99277			
0223972960	–	2.5	15.300	2.370	100.12453	9.83637			1.60
0223973200	I	113.2	15.600	0.070	100.12858	9.57811		22.20	1.30
0223973292	1.974	17.7	14.700	0.170	100.13010	9.51878	III	1.700	0.90
0223973318	I	1.0	15.600	2.600	100.13048	9.69152			
0223973692	3.456	14.6	15.700	1.760	100.13673	9.85833		2.700	0.90
0223974593	1.156	18.1	14.600	0.580	100.15134	9.31610	III		0.50
0223974689	–	1.8	14.800	1.100	100.15278	9.36818			
0223974891	1.212	2.9	12.900	1.740	100.15620	9.91617	III		2.10
0223975203	9.786	1.6	15.200	0.200	100.16160	9.36077	III		0.90
0223975253	–	10.5	12.600	1.440	100.16248	9.60013		3.500	0.60
0223975844	3.332	8.9	15.200	3.130	100.17236	9.90389	II	12.20	1.50
0223976028	I	4.1	13.400	0.710	100.17587	9.56050		7.300	1.70
0223976099	14.17	5.6	15.800	0.540	100.17683	9.53921	III	0.500	1.20
0223976494	2.267	12.7	14.300	0.800	100.18377	9.39887	III		1.10
0223976672	15.00	5.2	14.100	1.540	100.18687	9.96244	III	1.600	0.90
0223976747	3.173 AA	96.6	14.700	0.750	100.18816	9.47915		7.200	1.50
0223977051	4.53	5.5	15.200	1.410	100.19336	9.99640			
0223977092	–	0.5	14.000	2.000	100.19403	9.36149			
0223977232	0.712	0.8	14.300	0.340	100.19633	9.30929	III		
0223977953	4.919 AA	26.6	15.700	0.730	100.20782	9.61389	II	66.30	1.40
0223978227	3.779	20.7	16.000	2.890	100.21194	9.93148	III	2.300	0.80
0223978308	5.374 AA	5.6	15.400	3.650	100.21328	9.74633	II	3.500	1.80
0223978921	I	5.4	15.800	1.400	100.22346	9.55701		18.20	1.40
0223978947	8.5	0.2	13.600	1.340	100.22403	9.51095	III		1.80
0223979728	I	8.3	15.800	1.410	100.23665	9.63043		113.2	1.10
0223979759	3.84	0.6	15.400	3.770	100.23719	9.81144	III	3.900	1.60
0223979980	0.577	6.9	14.800	2.200	100.24097	9.94176	III		
0223980019	I	0.7	14.500	−0.500	100.24154	9.30101			
0223980048	12.5 AA	24.4	14.100	1.840	100.24200	9.61504	II	34.00	
0223980233	–	14.0	13.800	1.800	100.24457	9.60384		22.20	0.30
0223980258	6.990	8.9	14.900	0.980	100.24509	9.65531	II	27.90	0.60
0223980264	3.482 AA	54.0	14.600	0.960	100.24516	9.51607	II	14.30	1.90
0223980412	6.39	12.1	14.800	0.760	100.24764	9.99601	II	7.400	1.10
0223980447	1.675	9.2	16.000	1.220	100.24816	9.58649	II	6.400	0.90
0223980621	3.049	8.9	13.400	1.770	100.25099	9.98056	III	−1.200	1.80
0223980688	I	72.6	16.000	1.310	100.25205	9.75101		15.00	1.30
0223980693	5.282 AA	112.0	14.900	1.240	100.25214	9.48791	II	16.60	1.50
0223980807	I	8.1	14.600	1.790	100.25407	9.54585		6.400	
0223980941	3.794	85.9	15.300	1.800	100.25637	10.24905			
0223980988	8.58	1.6	15.400	0.000	100.25703	9.35170	III		
0223981023	7.320 AA	38.2	15.800	1.300	100.25770	9.64490		1.500	1.50

Table 2 – *continued*

CoRoT ID	Period (d)[a]	*AmpVar* (per cent)[b]	*R*	$B-V$	RA (J2000.0)	Dec. (J2000.0)	Memb-IR[c]	EW (Hα)[d]	Mass[e]
0223981174	1.974	19.7	15.600	1.000	100.26061	9.58235	III	0.600	1.50
0223981250	7.437	32.8	14.800	−0.200	100.26187	10.12015			
0223981285	1.152	1.0	15.300	2.300	100.26239	9.79856	III		
0223981349	8.014	13.4	15.000	2.300	100.26363	9.96535	III	1.500	0.80
0223981406	2.157	9.0	13.800	1.190	100.26449	9.52188	III	−2.500	1.60
0223981535	4.557	15.1	15.400	2.100	100.26640	9.96940	III	4.100	
0223981550	14.58	0.5	14.900	−2.200	100.26661	9.39267			1.20
0223981753	2.971	1.1	13.000	1.070	100.26965	9.60751	III		2.50
0223981811	I	86.4	15.900	4.140	100.27067	9.84631		36.50	1.60
0223982076	2.468	3.3	13.000	2.440	100.27471	9.45502	III	2.600	0.30
0223982136	3.018	10.7	14.700	1.280	100.27571	9.60653		10.00	1.40
0223982169	3.162	10.3	14.900	1.590	100.27621	9.49197	III	3.100	0.30
0223982299	4.671 AA	15.1	14.700	0.400	100.27850	9.03797			
0223982375	3.320	13.6	15.400	−0.200	100.27966	9.21076	II		
0223982407	2.582	23.6	14.600	1.310	100.28017	9.97540	III	1.400	1.10
0223982423	9.026	3.8	15.800	2.400	100.28040	10.22570			
0223982535	5.052	4.7	14.700	1.310	100.28240	9.73427	III		
0223982779	1.882	26.8	15.600	−2.000	100.28673	9.39554	III	2.400	0.60
0223982807	–	2.3	13.400	5.000	100.28716	10.23981	III		
0223983310	3.589	0.9	13.800	0.510	100.29544	10.01147	III		
0223983509	2.390	7.89	14.100	0.300	100.29829	10.04005			
0223983925	3.704	11.29	15.500	2.000	100.30511	9.91922		3.000	
0223984075	3.793	3.6	12.700	1.800	100.30750	9.92897	III	−2.600	
0223984253	10.42	9.6	16.000	1.530	100.31026	9.55614	III	1.900	1.10
0223984520	1.469	7.2	15.200	1.590	100.31425	9.77779	III	0.200	1.70
0223984572	I	14.5	12.300	2.400	100.31499	9.44282	III	5.500	0.30
0223984572	–	14.5	12.300	2.400	100.31499	9.44282	III		
0223984600	5.343	1.0	13.600	−0.300	100.31541	9.63857			
0223984608	6.098	7.7	10.200	3.180	100.31551	9.43795		1.900	1.20
0223985009	I	83.4	15.600	2.360	100.32182	9.90918	III	58.30	0.80
0223985176	6.547	8.3	15.700	1.240	100.32470	9.56046	III	2.900	0.60
0223985261	18.08 AA	20.3	15.400	1.280	100.32613	9.56501		28.90	1.40
0223985611	4.94	21.5	14.900	1.270	100.33174	9.52915	III	1.500	1.10
0223985845	2.604	9.4	15.900	1.220	100.33559	9.75999			
0223985987	3.308 AA	44.3	15.300	1.300	100.33751	9.56029	III	10.60	0.90
0223986498	3.206	6.5	14.800	1.680	100.34600	9.45753	III		
0223986686	–	0.6	11.900	0.090	100.34904	9.56587	II		
0223986811	7.92	2.7	15.700	1.020	100.35109	9.53181	III		
0223986923	8.300	0.8	15.200	1.160	100.35297	9.43999			
0223987178	9.84 AA	36.8	15.600	0.850	100.35670	9.57878	III	15.90	0.60
0223987553	1.544	22.3	14.300	0.480	100.36308	9.58516	III	1.100	1.50
0223987997	6.456	22.9	13.800	0.020	100.36986	9.64432	II		
0223988020	–	1.0	14.200	−0.200	100.37021	10.15428	III		
0223988099	–	2.5	13.700	0.660	100.37155	9.66014	II	−1.400	1.60
0223988099	3.273	2.5	13.700	0.660	100.37155	9.66014		−1.400	1.60
0223988742	5.025	16.7	15.300	1.270	100.38172	9.80926		5.200	1.60
0223988827	4.767	9.3	15.800	0.810	100.38329	10.00690	III	13.10	1.10
0223988965	9.5	4.5	14.200	0.640	100.38538	9.63550	III	1.300	0.90
0223989567	I	8.4	15.200	1.700	100.39403	9.60913	III	4.500	0.50
0223989989	6.547	7.2	15.900	0.800	100.40102	9.65579	III	1.600	0.80
0223990299	4.469	9.3	14.500	0.660	100.40536	9.75196		35.00	1.20
0223990764	–	0.6	15.800	3.200	100.41270	9.49399	III		
0223990964	10.17 AA	11.5	13.600	0.340	100.41553	9.67456	II	52.50	1.60
0223991355	–	0.9	12.700	0.000	100.42163	9.54543			
0223991789	3.956	11.7	14.600	0.560	100.42803	9.71584	II	0.900	0.60
0223991832	8.608	18.2	16.000	−0.100	100.42868	9.41913			
0223991967	–	0.1	12.500	0.650	100.43058	9.45033	III		
0223992383	3.380	5.1	15.200	0.310	100.43725	9.74473	II		0.80
0223992685	18.5	0.7	12.300	0.300	100.44153	9.39736			
0223993084	6.456	5.3	15.400	−0.140	100.44751	9.70001	III	2.600	0.50
0223993180	2.411	1.4	12.900	0.430	100.44890	9.86750	III		1.80
0223993199	I	40.3	14.200	0.740	100.44914	9.56957	III		

Table 2 – *continued*

CoRoT ID	Period (d)[a]	*AmpVar* (per cent)[b]	*R*	$B-V$	RA (J2000.0)	Dec. (J2000.0)	Memb-IR[c]	EW (Hα)[d]	Mass[e]
0223993277	1.184	3.9	13.200	0.110	100.45027	9.71222	III		1.50
0223993499	I	0.9	14.500	3.200	100.45351	9.72045			1.70
0223993840	3.250	35.8	14.500	1.050	100.45837	9.49241	III		0.90
0223994268	3.762	4.9	13.200	0.240	100.46436	9.89531			1.50
0223994721	I	37.9	14.200	0.110	100.47102	9.96762	III		0.80
0223994760	5.634	8.9	14.800	0.580	100.47147	9.84660	III	1.800	1.10
0223995167	–	0.4	13.300	2.000	100.47691	9.48783			
0223995308	10.5 AA	53.6	15.800	−0.130	100.47881	9.71481	II		0.30
0223995327	–	0.8	13.200	0.230	100.47910	9.89077			
0223997570	3.660	6.5	14.500	0.670	100.51064	9.61480			
0223997608	–	2.7	14.700	0.260	100.51109	9.97452			
0223998980	–	2.2	15.500	0.600	100.52973	9.89573	III		
0223999063	–	0.3	11.700	0.410	100.53070	9.82991			
0223999581	–	0.5	14.200	1.220	100.53790	9.98422			
0223999591	–	1.2	15.700	0.500	100.53800	9.80151			
0224000646	–	0.5	13.700	0.900	100.55241	9.98546			
0224000835	–	1.3	15.700	−0.400	100.55477	9.76773			
0224001158	I	5.8	15.700	−0.300	100.55867	9.59576			
0224001312	–	1.0	14.200	−0.150	100.56084	9.84115			
0224003566	–	0.5	14.700	−0.200	100.59132	9.80927			
0224006123	10.25 AA	53.2	13.000	0.400	100.62704	9.15735			
0400007328	2.434	23.0	13.530	2.450	100.32380	9.49061	III	2.400	0.30
0400007394	3.443	4.6	14.020	3.020	100.21672	9.75134		2.800	0.50
0400007528	9.42	14.0	14.450	1.860	100.15780	9.58167	II	23.40	0.30
0400007529	4.842	9.3	14.560	2.250	100.21948	9.73917	III	2.200	0.40
0400007538	I	23.1	14.450	0.230	100.15217	9.84601		21.10	0.40
0400007614	I	13.6	14.640	1.580	100.05709	9.94183		130.2	0.40
0400007686	I	5.1	15.150	−8.100	100.27679	9.47745		56.10	0.40
0400007687	11.5	5.6	15.220	1.700	100.30544	9.86512	III	2.000	0.50
0400007702	5.884	20.2	15.230	1.550	100.15916	9.49792	II	2.600	0.50
0400007709	–	10.3	14.950	1.720	100.35226	9.62654		8.900	0.30
0400007734	9.996	5.6	15.200	1.830	100.36250	9.50365		25.80	0.50
0400007743	–	0.9	15.230	1.910	100.37020	9.58169			
0400007765	I	2.7	15.300	1.840	100.23683	9.86573		1.100	0.30
0400007784	9.114	6.1	15.350	1.480	100.00467	9.59265	III		
0400007786	8.608	6.7	15.460	1.180	100.21748	9.94537		3.100	0.50
0400007803	9.73	12.3	14.680	1.130	100.26503	9.50806	II	20.40	
0400007809	3.990	14.7	15.510	1.510	100.12186	9.73542		31.30	0.40
0400007860	2.172	1.8	15.280	0.810	100.23959	9.82246	III		
0400007889	1.897	46.3	15.190	1.810	100.27310	9.52793		3.000	0.30
0400007919	4.625	15.0	15.620	1.600	100.26164	9.38756			
0400007955	I	17.1	15.900	1.380	100.21982	9.71679		19.40	0.30
0400007956	1.260	3.6	15.330	1.580	100.27903	9.68180	III	2.800	
0400007957	I	16.9	15.820	1.680	100.32107	9.54786		2.100	0.30
0400007959	5.738	15.5	15.600	0.970	100.27805	9.79100	II	6.200	
0400008031	–	29.3	15.840	1.110	100.26287	9.48460		14.60	
0400008086	5.34	3.4	15.890	1.000	100.23363	9.71502		8.000	
0400008126	0.546	1.7	15.540	0.970	100.29521	9.88840	III	13.20	
0500007008	–	5.3	10.350	1.180	100.15522	9.79159			
0500007018	1.487	1.0	10.950	1.360	100.02357	9.59702	III		
0500007021	–	0.3	10.720	1.010	100.48482	9.83499			
0500007022	3.332	5.6	11.050	1.310	100.30433	9.45886	III		
0500007025	0.747	7.9	11.360	1.230	100.19200	9.82149	III		3.00
0500007031	–	0.8	11.450	0.820	100.19658	9.48052			
0500007038	4.132	0.8	11.880	1.060	100.15281	9.78959	III		
0500007039	11.92	0.6	11.980	1.140	100.27870	9.38927	III	−1.500	2.20
0500007046	I	3.6	12.550	1.470	100.18600	9.80059		48.90	
0500007051	10.0	1.1	11.890	0.700	100.25919	9.86443	III	−1.600	2.10
0500007087	14.0	2.0	12.340	0.360	100.09639	9.93886	III		
0500007089	I	21.4	12.320	0.260	100.30362	9.43746		85.60	1.70
0500007115	1.995	35.5	13.420	1.050	100.30241	9.87533	II	35.30	
0500007120	8.53	14.2	13.450	1.010	100.19793	9.82471	II	12.80	1.80

Table 2 – *continued*

CoRoT ID	Period (d)[a]	*AmpVar* (per cent)[b]	R	$B-V$	RA (J2000.0)	Dec. (J2000.0)	Memb-IR[c]	EW (Hα)[d]	Mass[e]
0500007122	I	57.2	12.780	0.290	100.37966	9.44951		25.90	
0500007126	–	0.6	12.550	−0.040	100.23119	9.52272			
0500007137	2.914	7.6	12.780	0.020	100.29095	9.45339	III	3.100	1.20
0500007157	4.344	7.2	13.190	0.260	100.25324	9.85620	III	1.600	1.30
0500007176	4.024	6.9	13.400	0.330	100.26849	9.85725	III		
0500007197	9.114	5.0	13.570	0.220	100.18063	9.84988	III	1.700	0.80
0500007202	–	0.3	13.650	0.260	100.20934	9.33399			
0500007209	I	45.2	13.600	0.170	100.21081	9.91593		11.20	1.60
0500007217	2.582	10.4	13.520	0.000	100.27172	9.88772	III	1.500	
0500007221	I	9.3	13.430	−0.130	100.29939	9.44207		5.400	0.70
0500007227	7.151	6.9	13.880	0.280	100.12758	9.76962	III	1.500	1.30
0500007248	7.50	2.5	13.860	0.170	100.27125	9.86238	III	1.700	1.10
0500007249	I	5.9	14.680	0.980	100.41155	9.53661		58.60	1.20
0500007252	13.88	39.8	13.730	0.000	100.16299	9.84962	II	46.50	1.50
0500007269	3.674	92.7	14.530	0.740	100.17435	9.86237	II	22.90	1.10
0500007272	3.748	14.9	13.380	−0.420	100.16840	9.84735	III	58.30	0.70
0500007276	4.743	7.2	13.970	0.150	100.17261	9.80267		2.400	1.10
0500007283	3.217	9.6	13.940	0.100	100.23215	9.85385	II	8.000	1.00
0500007298	15.25	4.3	14.070	0.150	100.15262	9.80638	III	4.900	1.10
0500007300	I	0.7	13.480	−0.450	100.15151	9.37904			
0500007308	3.141	9.3	14.200	0.230	100.10616	9.80721	III	0.800	1.10
0500007315	7.812 AA	32.9	13.920	−0.080	100.17216	9.85066	II	24.50	0.80
0500007330	4.304	3.5	14.030	−0.030	100.27422	9.87996	III	0.900	0.80
0500007335	14.99 AA	8.8	14.020	−0.070	100.26789	9.41449	II	101.8	0.60
0500007347	4.206	15.3	14.210	0.060	100.25000	9.48057	III	1.700	0.80
0500007354	1.165	11.6	14.240	0.050	100.22991	9.84718		2.800	1.00
0500007366	3.617	8.2	14.060	−0.190	100.19733	9.81373	III	1.800	0.50
0500007369	I	15.2	13.590	−0.680	100.27808	9.57943		49.40	
0500007379	14.17	2.7	14.300	−0.010	100.17095	9.79936		7.500	0.80
0500007383	1.289	4.8	13.970	−0.360	100.27368	9.90520	III	3.800	0.50
0500007410	–	2.8	14.050	−0.390	100.21897	9.86833		6.900	0.70
0500007416	3.748	3.5	14.170	−0.300	100.27124	9.81332	III		
0500007457	1.049	3.0	14.480	−0.130	100.17415	9.83120	III	4.200	0.60
0500007458	4.625	5.8	14.490	−0.130	100.18768	9.76162		2.400	0.80
0500007460	8.49 AA	42.0	14.600	−0.030	100.18006	9.78535	II	27.10	0.90
0500007473	I	24.9	14.430	−0.260	100.22610	9.82232		161.1	0.50
0500007505	I	8.3	14.900	0.070	100.17086	9.46509		13.20	
0500007550	–	0.4	14.590	−0.440	100.40549	9.53271			
0500007556	3.405	4.5	14.250	−0.810	100.34229	9.35863	III	3.800	
0500007572	8.08	3.2	14.440	−0.670	100.29298	9.36376	III	2.700	
0500007580	1.805	17.5	14.700	−0.450	100.24931	9.86359	III	4.900	0.40
0500007585	9.786	14.3	14.780	−0.410	100.19170	9.29951			
0500007610	9.34	17.4	14.690	−0.610	100.24792	9.49770	II	26.20	0.30
0500007634	11.25	6.7	14.970	−0.410	100.26488	10.00983		6.900	0.50
0500007667	5.405	22.6	15.190	−0.340	100.31035	9.62065	III	4.100	
0500007682	I	7.9	14.580	−1.010	100.31008	9.44952		2.700	0.30
0500007708	9.584	11.4	15.220	−0.450	100.22546	9.49752	III	3.600	
0500007727	I	20.7	15.150	−0.590	100.29583	9.59881		61.50	0.80
0500007730	12.5	3.2	14.850	−0.910	100.20505	9.96077		50.80	0.50
0500007752	4.042	5.4	14.720	−1.110	100.28734	9.56278	II	51.00	0.30
0500007766	I	7.2	15.070	−0.800	100.29283	9.55696		2.700	0.30
0500007770	10.0	4.4	15.300	−0.580	100.01115	9.69690	III		
0500007794	8.854	7.1	15.410	−0.530	100.23939	9.48984	III	4.000	
0500007808	5.025	2.9	15.060	−0.920	100.29496	9.77811	III	3.900	0.30
0500007816	7.378	1.1	15.060	−0.980	100.22344	9.78455	II	8.100	0.30
0500007837	I	19.5	15.380	−0.740	100.28690	9.88365			
0500007857	I	8.0	15.360	−0.820	100.26905	9.64190		108.0	0.30
0500007874	I	3.3	15.740	−0.500	100.18720	9.81921		2.600	
0500007896	9.296	14.0	14.950	−1.360	100.27596	9.41769	II	34.70	0.20
0500007918	I	2.7	15.330	−1.070	100.14539	9.90200		5.200	0.30
0500007930	6.30	19.8	15.620	−0.810	100.18580	9.54061		60.00	0.30
0500007939	1.029	5.3	15.430	1.200	100.24333	9.45696	III	6.700	

Table 2 – *continued*

CoRoT ID	Period (d)[a]	*AmpVar* (per cent)[b]	*R*	$B-V$	RA (J2000.0)	Dec. (J2000.0)	Memb-IR[c]	EW (Hα)[d]	Mass[e]
0500007963	2.568	28.6	15.880	−0.660	100.19968	9.55087			
0500007992	2.318	2.4	15.170	−1.480	100.19115	9.64566	III	4.100	
0500008003	3.19	5.0	15.630	−1.070	100.35450	9.60005	III		
0500008007	1.805	4.4	15.900	−0.820	100.17437	9.69406		3.100	
0500008038	3.469	6.7	15.660	−1.150	100.10687	9.99993	II		0.30
0500008049	10.44	26.4	15.430	−1.420	100.32468	9.48364	II	231.4	0.40
0500008061	–	6.8	15.650	−1.230	100.32534	9.64038		32.50	0.30
0500008064	I	0.8	15.930	−0.970	100.22479	9.84946			
0500008145	4.448	5.2	15.620	−1.590	100.16884	9.58365	II		
0500008156	–	20.7	15.880	−1.360	100.30215	9.58578			
0500008183	7.67	3.5	15.740	−1.610	100.27488	9.65395	II	7.400	0.20
0500008192	2.408	12.1	15.760	−1.620	100.30569	9.63716	II		
0500008211	2.324	3.6	15.770	−1.700	100.26266	9.62660	II	34.10	0.50
0500008213	4.364	3.9	15.880	−1.600	100.27111	9.82302	II	8.300	

[a]I indicates irregular variables, AA indicates AA Tau-type stars.
[b]Short term variability amplitude of the LCs.
[c]Membership-IR classification (Class II and Class III) of Sung et al. (2009), considering also other membership criteria listed in Sung et al. (2008).
[d]Hα EW from Lamm et al. (2004).
[e]Masses are from the Siess et al. (2000) tracks. Stars were placed in the $T_{\rm eff}$, $L_{\rm bol}$ diagram converting spectral types to $T_{\rm eff}$ and *I* band and (in absence of the *I* magnitude) *V*-band bolometric corrections, using Kenyon & Hartmann (1996).

reduction and analysis. In brief, we prepared the LCs by correcting the following systematic effects: spurious data points (mainly due to cosmic rays and/or to the satellite crossing of the South Atlantic anomaly), as flagged by the reduction pipeline were removed; we rebinned the data to 2 h to smooth out the orbital period of the satellite (1.7 h); spurious long period trends (due to pointing and instrumental drift) were removed by fitting a third degree polynomial to the data and then dividing the original data points by this function.

The presence of periodic signals was detected using the Lomb Normalized Periodogram (LNP) technique (Scargle 1982; Horne & Baliunas 1986). With this algorithm we calculated the normalized power $P(\omega)$ as function of angular frequency $\omega = 2\pi\nu$ and identified the location of the highest peak in the periodogram. In order to decide the significance of the peak we have followed Eaton, Herbst & Hillenbrand (1995), randomizing the temporal bins from the original LC. By calculating the maximum power on a large number of randomized data sets, the conversion from power to False Alarm Probability (FAP) can be determined. In detail, we constructed 1000 LCs *resampled* from the original ones randomizing the position of blocks of adjacent temporal bins (block length, 12 h; e.g. Flaccomio et al. 2005). By shuffling the data we break any possible time correlation and periodicity of the LC on time-scales longer than the block duration. We calculated the Scargle periodogram for all the randomized LCs and we compared the maximum from the real periodogram to the distribution obtained from the randomized LCs, at the same frequency, in order to establish the probability that values as high as the observed one are due to random fluctuations. Given some threshold FAP_* we state that the detected candidate periodicity is statistically not significant if $\mathrm{FAP} > \mathrm{FAP}_*$. The calculation we performed on *CoRoT* LCs led often to small FAPs, indicating that LNPs of our LCs present peaks that in most cases cannot be explained by pure stochastic noise, or non-periodic variability on time-scales shorter than 12 h. In fact, if LCs present variations on time-scale smaller than the size of the temporal block we used in the simulations, these variations will be still present in the simulated curves and will be not recognized as significant (more details in Affer et al. 2012). We have chosen a bin size of 12 h as a reasonable compromise between the expected time-scale of stochastic variations and the shortest expected periodic signal. Once significant peaks (at FAP 1 per cent; since we simulated 1000 LCs, the 1 per cent FAP power is the power that was exceeded by the highest peak in 10 simulations) were determined from the LNPs, we also used an autocorrelation analysis (Box & Jenkins 1976) to validate the periodicity of the LCs and to eliminate or correct spurious periods due to aliasing effects (in 5 per cent of the cases, with a 95 per cent confidence interval) or residual effects due to the choice of temporal blocks used in the LCs' simulations (block length, 12 h).

Autocorrelation takes each point of the LC measured at time t and compares the value of that point to another at time $t + L$. Points separated by L will have very similar values if the data contained some variability with period L; thus, the autocorrelation function will have peaks corresponding to periods of variability in the data. The autocorrelation $r_{\rm L}$ of a sample population X as a function of the lag L is

$$r_{\rm L} = \frac{\sum_{k=0}^{N-L-1}(x_k - \bar{x})(x_{k+L} - \bar{x})}{\sum_{k=0}^{N-1}(x_k - \bar{x})^2},$$

where $\bar{x}$ is the mean of the sample population X and N is the sample size, the quantity $r_{\rm L}$ is called the autocorrelation coefficient at lag L. The correlogram for a time series is a plot of the autocorrelation coefficients $r_{\rm L}$ as a function of L. A time series is random if it consists of a series of independent observations with the same distribution. In this case, we would expect $r_{\rm L}$ to be statistically not significant for all values of L. We have chosen to adopt a 95 per cent confidence level to select significant autocorrelation coefficient.

Following Alencar et al. (2010), morphologically we can divide the LCs in four groups: (1) spot-like periodic LCs, whose periodicity can be interpreted as rotational modulation of surface features such as cool and/or hotspots (Fig. 3, top-left panel); (2) AA Tau-like systems, whose quasi-periodicity is likely caused by the obscuration of the stellar photosphere by circumstellar disc material (Fig. 3, top-right panel), the stability of the spot-like LCs on the time-scale of the observations, makes them easily distinguishable from the AA Tau-like ones; (3) irregular LCs, whose non-periodic brightness modulations (some of them with peak-to-peak variations up to 1 mag) are probably due to a complex mixing of non-steady

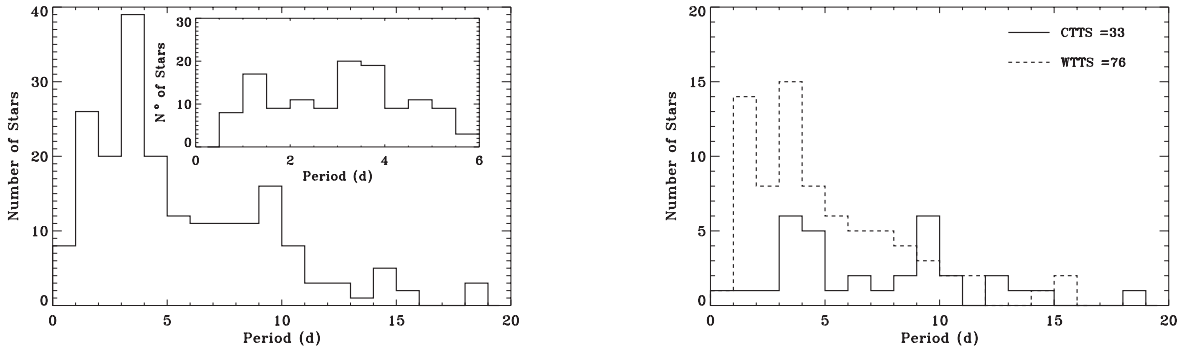

Figure 5. Left-hand panel: rotational period distribution for NGC 2264 members, the inset plot is the same diagram but zoomed into the period region between 0 and 6 d. Right-hand panel: rotational period distributions for CTTSs (solid line) and for WTTSs (dashed line).

accretion phenomena, and obscuration by non-uniformly distributed circumstellar material, as suggested by Alencar et al. (2010) (Fig. 3, bottom-left panel); and (4) non-variable LCs which do not display an obvious periodicity, most of which look like noisy LCs with small variability amplitude $\leq$1 per cent (Fig. 3, bottom-right panel).

To evaluate a short term variability amplitude of the LC, we calculated the running median flux, obtained using a temporal bin set up by 15 time points (thus, a time-scale of 15×512 s), we calculated for each time value the difference between the instantaneous flux and the running median flux derived at the corresponding time, obtaining an array. We measured the amplitude variation of the LC as the difference between the maximum and the minimum values of this array. We found that the variability amplitude range is 2 to 171 per cent for CTTSs and 1.0 to 38 per cent for WTTSs in our sample. In Fig. 4, we show the results of the complete analysis for two LCs, one belonging to a CTTS and the other to a WTTS.

4 RESULTS: ROTATIONAL PERIODS

Of the 301 monitored cluster members, we found that 189 are periodic variables, with regular LCs, possibly resulting from the rotational modulation of the light by stellar spots, 20 are AA Tau-like systems, 45 are irregular LCs and 47 display no significant variability (noise dominated LCs). Among the 86 WTTSs, we measured periods for 76 stars (74 regular and 2 AA Tau like), 6 were found to be irregular and 1 non-variable. For 3 stars we did measure a period, the variability is clearly due to spot, nonetheless we discarded these periods as they are not significant according to both the LNP and autocorrelation methods. Among the 59 CTTSs, we measured periods for 33 stars (21 regular and 12 AA Tau like), 23 were found to be irregular and 1 non-variable, for two stars the periods found were discarded as not significant. In Table 1, we list the samples used in this work, indicating the morphological division performed (spot like, AA Tau like, etc.) and the membership-IR classification (Class II and Class III) following Sung et al. (2009).

All the rotational periods derived for NGC 2264 members are reported in Table 2. For each star we list: the *CoRoT* ID; the derived period; the variability amplitude *AmpVar*; the *R* magnitude; the $B-V$ magnitude; the RA and Dec.; the membership-IR classification (Class II and Class III) following Sung et al. (2009) and other membership criteria listed in Sung et al. (2008); the Hα EWs from Dahm & Simon (2005) and the mass from the Siess, Dufour & Forestini (2000) tracks.

In the left-hand panel of Fig. 5, we show the rotational period distribution for NGC 2264 members, while the distribution of rotational periods for CTTSs and WTTSs is shown in the right-hand panel. Although the statistics are limited, it is evident that the period distribution of the CTTSs looks quite different from that of the WTTSs, with CTTSs being slower rotators on average (median $P_{\rm Rot} = 7.0$ d) with respect to WTTSs (median $P_{\rm Rot} = 4.2$ d), in the cluster NGC 2264. According to a Kolmogorov–Smirnov (KS) test (Press et al. 2002), there is only a probability of 2 per cent that the two distributions are equivalent.

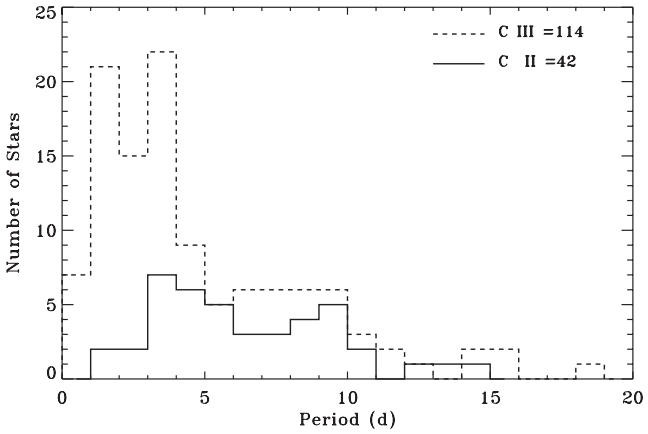

Figure 6. Rotational period distribution for Class II (dashed line) and Class III members (solid line). The two classes were selected following the membership-IR classification of Sung et al. (2009) and other membership listed in Sung et al. (2008).

The peaks of the distribution for CTTSs are located at about $P =$ 3–5 and 9 d. WTTSs distribution suggests two peaks at $P =$ 3–5 and 1−2 d. The difference is even more evident if we compare the period distributions of Class II and Class III stars, as is shown in Fig. 6. We selected Class II and Class III members following the membership-IR classification of Sung et al. (2009), using the four *Spitzer* IRAC bands and other membership criteria listed in Sung et al. (2008). For Class II-Class III members the KS test yields a probability of 0.2 per cent that the two distributions are drawn from the same parent population. The observed rotational period distributions are in agreement with the conclusion derived by the ground-based study of Lamm et al. (2005), on the accretion–rotation relationship, that is, differences do exist in the rotational behaviour of accreting and non-accreting stars.

Fig. 7 shows rotation period plotted as a function of stellar mass, derived from the Siess et al. (2000) tracks. The diagram shows no clear trend of rotation period with stellar mass. We calculated the period distributions in three mass intervals: $M < 0.75$ ('low'); $0.75 < M < 1.55$ ('mid'); $1.55 < M < 3.0\,{\rm M}_{\odot}$ ('high'). Using a KS

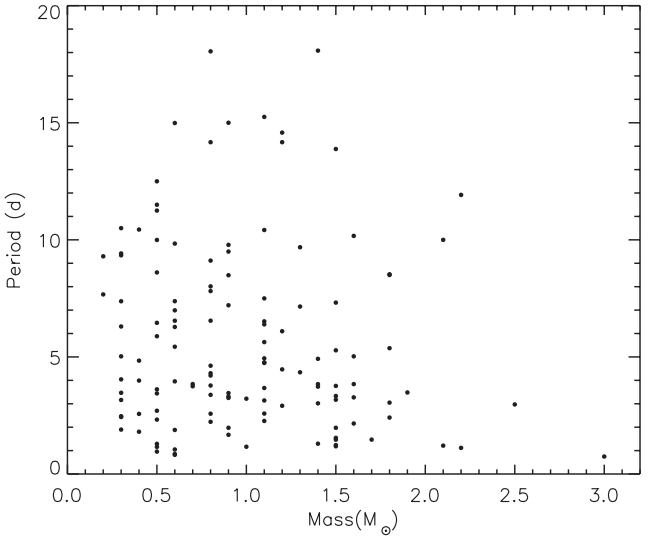

Figure 7. Rotation period as a function of stellar mass for our sample. The mass values are derived from the Siess et al. (2000) tracks.

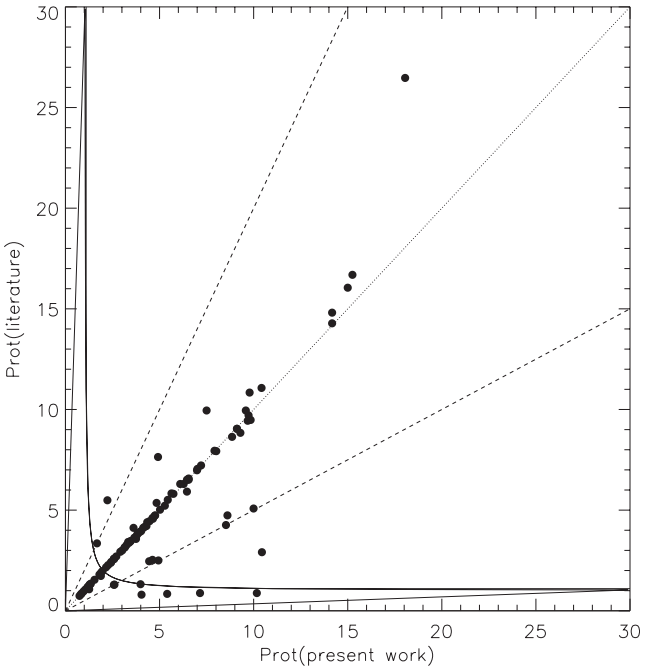

Figure 8. Comparison between the periods derived in this study and the ones derived by Lamm et al. (2004) for the sample stars in common. Stars with the same period in the two studies are located on the bisector (dotted line). The two dashed lines on each side of the bisector represent harmonics (0.5–2.0 P). The solid curves show the loci of the 1 d^{-1} aliases.

test, we have verified that the probabilities that the 'low' and 'mid', the 'low' and 'high', and the 'mid' and 'high' distributions are equivalent are 91 per cent, 58 per cent and 54 per cent, respectively, neither of which can lead us to infer that they are significantly different. The median periods are 4.8, 4.5 and 3.5 d for the 'low', 'mid' and 'high' samples, respectively.

We now compare the periods derived from the *CoRoT* data with those of Lamm et al. (2004, 2005), who identified 405 periodic variables and 184 irregular variable members. We analysed the 103 NGC 2264 members in common with the Lamm et al. (2004) ones. The *CoRoT* periods derived in this study and ground-derived ones (Lamm et al. 2004), apart from the presence of few aliases, are comparable with the exception of the 1 d periods derived from ground, likely affected by the day–night alternance (*CoRoT* LCs have both a better sampling and time coverage than Lamm et al. 2004 ones). A scatter plot of the *CoRoT* versus ground periods is shown in Fig. 8. We followed the indications of Lamm et al. (2004) to estimate the error in the measured periods, which is related to the finite frequency resolution $\delta\nu$ of the power spectrum. In our study, we take advantage of the uniformity of *CoRoT* sampling; thus, the frequency resolution is related to the total time span T of the observations (23 d) with $\delta\nu \approx 1/T$ (Roberts, Lehar & Dreher 1987). Thus, we assume as typical error in the period, that is given by $\delta P \approx (\delta\nu P^2)/2$. We found that for period shorter than 10 d, the estimated error is $\leq$20 per cent, while it grows with period. With these indications, we find that 83 per cent (85/103) of the sample stars have consistent periods in the two survey, most of the inconsistent values lie along either harmonics (9/103) or the 1 d aliases curve (5/103).

We compare ground and *CoRoT* data for few intriguing cases, in Fig. 9 we reported a LC of a star with short period illustrating the quality of the *CoRoT* LC with respect to the ground one. In Fig. 10, we show the folded LC from Lamm et al. (2004) together with the *CoRoT* one, for a case in which the ground determination of 0.84 d is clearly wrong, in comparison with the *CoRoT* determination of 5.5 d. This comparison highlights the usefulness of a continuous temporal coverage, as can only be achieved from space.

5 SUMMARY AND CONCLUSIONS

We performed an accurate study of rotation periods in the young open cluster NGC 2264, based on the very accurate *CoRoT* photometry, also to search for a correlation between accretion and stellar rotation. We derived rotational period for 209 cluster members, out of 301, which are found to be periodic variables, with a spot-like modulation of their light or AA Tau like.

This work enabled us to study the distribution of rotational periods of CTTSs and WTTSs. In order to overcome the bias introduced by the use of NIR excess to classify CTTSs, we used Hα EWs. Furthermore, the clean and continuous LCs of *CoRoT* allowed us to avoid problems due to discontinuous time sampling. Thanks to the high quality of the *CoRoT* LCs, our results provide the most complete set of rotational periods of NGC 2264 members, to date, compared to ground-based data.

As discussed in Section 1, several models assume that accreting stars may be locked to their discs by strong magnetic fields that channel streams accretion (Shu et al. 1994; Hartmann 2002). This would result in slower rotation velocities for CTTS, compared to WTTS which have no inner discs, and some observations suggested differences up to a factor of 2 in rotational velocities of CTTS versus WTTS in Taurus (Edwards et al. 1993). However, several other studies have found no significant variations between rotational velocities of CTTS and WTTS in ONC and IC 348 (Stassun et al. 1999; Rhode, Herbst & Mathieu 2001; Cieza & Baliber 2006). These results seem to suffer from several biases affecting the selected samples and even the disc and accretion indicators adopted. These differences may also be due to a classification problem, on what one defines classical and weak line T-Tauri stars.

We found that the rotational distributions of CTTSs and WTTSs are different, with WTTSs rotating faster, with a median $P_{\rm Rot}$ =

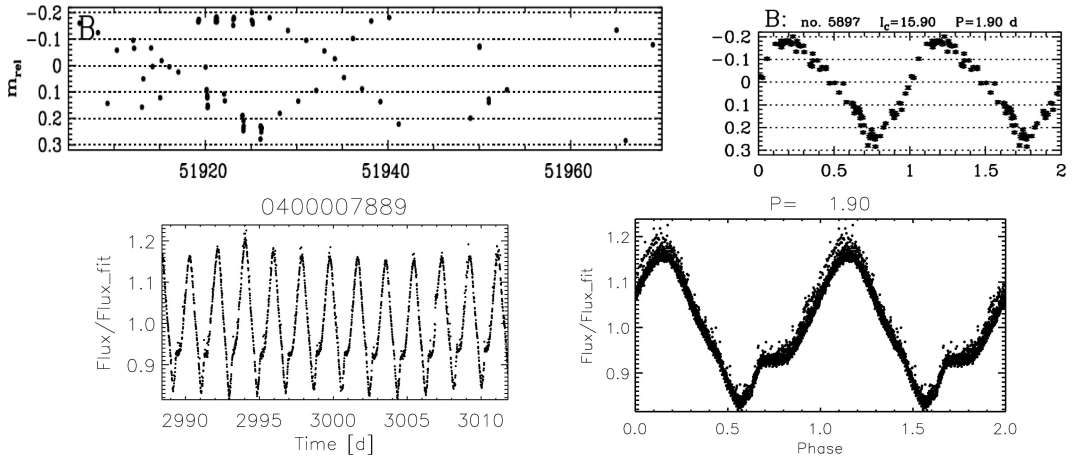

Figure 9. LC obtained from ground observations (Lamm et al. 2004, upper-left panel, between 2000 December 30 and 2001 March 01) and the folded LC (upper-right panel). *CoRoT* LC for the same star (lower-left panel) and folded LC (lower-right panel). The derived periods are indicated on the top of each folded LC panel, and are in agreement. Time in the *CoRoT* LC (bottom-left panel) is in days from 2000 January 01 (JD-245 1544.5).

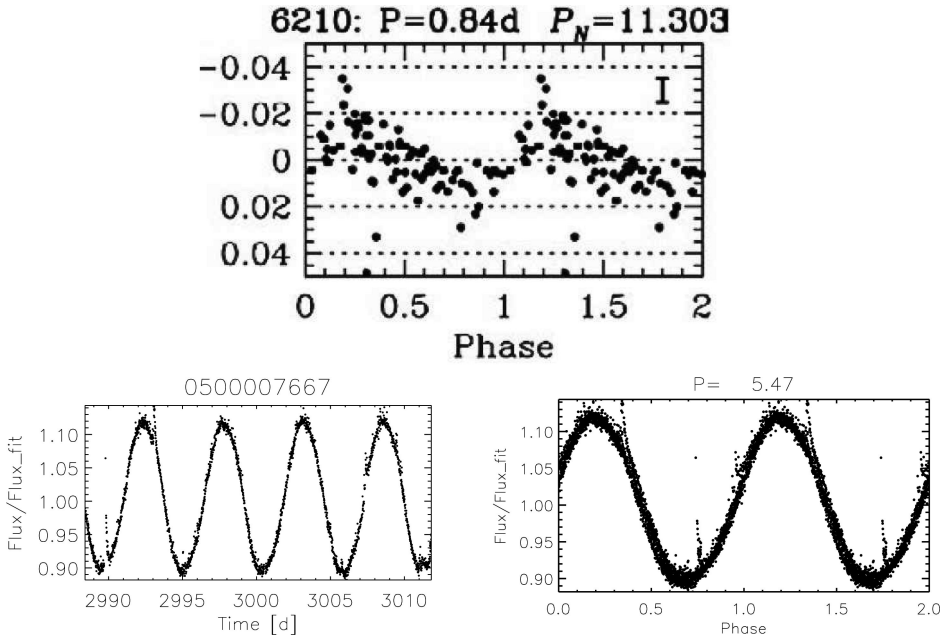

Figure 10. Folded LC from Lamm et al. (2004) (top panel) with the CoRot LC and folded LC (bottom panel). In this case, the ground determination of 0.84 d is clearly wrong, compared with the *CoRoT* determination of 5.5 d. Time in the *CoRoT* LC (bottom-left panel) is in days from 2000 January 01 (JD-245 1544.5).

4.2 d, with respect to CTTSs, with a median $P_{\rm Rot} = 7.0$ d. Our results are even more significant using a Class II–Class III comparison, probably because of the better statistics. This could suggest that the presence of accretion, or any other properties related to star–disc interaction, affects the rotational period. It is consistent with the disc-locking scenario (Shu et al. 1994; Hartmann 2002) and agrees with previous results in ONC (Choi & Herbst 1996; Herbst et al. 2002; Rebull et al. 2005), also confirming the previous conclusions of Lamm et al. (2005) and Cieza & Baliber (2007) for NGC 2264.

A new extensive multiband campaign has been executed on NGC 2264 in 2011 December (*CoRoT*+*Spitzer*+*Chandra* complemented with *MOST* observations). The new data will enable us to tackle some open questions, on the subject of this paper, such as the stability of the disc structure responsible for the AA Tau-like variability or differential rotation and the possibility of detecting period changes, when spots evolve and appear at different latitudes.

ACKNOWLEDGMENTS

LA and GM acknowledge support from the ASI-INAF agreement I/044/10/0. We wish to thank the anonymous referee for his/her careful reading of the manuscript and for the suggestions to improve the paper.

REFERENCES

Affer L., Micela G., Favata F., Flaccomio E., 2012, MNRAS, 424, 11
Aigrain S., Irwin M., 2004, MNRAS, 350, 331
Alencar S. H. P. et al., 2010, A&A, 519, A88
Baglin A. et al., 2006, in 36th COSPAR Scientific Assembly, p. 3749
Barrado y Navascués D., Martín E. L., 2003, AJ, 126, 2997
Bouvier J., 2008, A&A, 489, L53
Bouvier J., 2009, EAS Publ. Ser., 39, 199

Bouvier J., Cabrit S., Fernandez M., Martin E. L., Matthews J. M., 1993, A&A, 272, 176
Bouvier J. et al., 1999, A&A, 349, 619
Bouvier J. et al., 2003, A&A, 409, 169
Bouvier J. et al., 2007, A&A, 463, 1017
Box G. E. P., Jenkins G. M., 1976, Holden-Day Series in Time Series Analysis. Holden-Day, San Francisco
Camenzind M., 1990, Rev. Mod. Astron., 3, 234
Choi P. I., Herbst W., 1996, AJ, 111, 283
Cieza L., Baliber N., 2006, ApJ, 649, 862
Cieza L., Baliber N., 2007, ApJ, 671, 605
Collier Cameron A., Campbell C. G., Quaintrell H., 1995, A&A, 298, 133
Dahm S. E., 2008, in Reipurth B., ed., ASP Monograph Publ. Vol 4, Handbook of Star Forming Regions: Vol. I, The Northern Sky. Astron. Soc. Pac., San Francisco, p. 966
Dahm S. E., Simon T., 2005, AJ, 129, 829
Dahm S. E., Simon T., Proszkow E. M., Patten B. M., 2007, AJ, 134, 999
Eaton N. L., Herbst W., Hillenbrand L. A., 1995, AJ, 110, 1735
Edwards S. et al., 1993, AJ, 106, 372
Flaccomio E., Micela G., Sciortino S., Feigelson E. D., Herbst W., Favata F., Harnden F. R. Jr, Vrtilek S. D., 2005, ApJS, 160, 450
Flaccomio E., Micela G., Sciortino S., 2006, A&A, 455, 903
Flaccomio E., Micela G., Favata F., Alencar S. P. H., 2010, A&A, 516, L8
Fűrész G. et al., 2006, ApJ, 648, 1090
Grosso N., Bouvier J., Montmerle T., Fernández M., Grankin K., Zapatero Osorio M. R., 2007, A&A, 475, 607
Hartmann L., 2002, ApJ, 578, 914
Hartmann L., MacGregor K. B., 1982, ApJ, 259, 180
Herbst W., Rhode K. L., Hillenbrand L. A., Curran G., 2000, AJ, 119, 261
Herbst W., Bailer-Jones C. A. L., Mundt R., Meisenheimer K., Wackermann R., 2002, A&A, 396, 513
Horne J. H., Baliunas S. L., 1986, ApJ, 302, 757
Kenyon S. J., Hartmann L., 1995, ApJS, 101, 117
Kenyon S. J., Hartmann L., 1996, VizieR Online Data Catalog, 2101, 10117
Koenigl A., 1991, ApJ, 370, L39
Lamm M. H., Bailer-Jones C. A. L., Mundt R., Herbst W., Scholz A., 2004, A&A, 417, 557
Lamm M. H., Mundt R., Bailer-Jones C. A. L., Herbst W., 2005, A&A, 430, 1005
Martín E. L., 1998, AJ, 115, 351
Matt S., Pudritz R. E., 2005, ApJ, 632, L135
Matt S. P., Pinzón G., de la Reza R., Greene T. P., 2010, ApJ, 714, 989
Matt S. P., Pinzón G., Greene T. P., Pudritz R. E., 2012, ApJ, 745, 101
Ménard F., Bouvier J., Dougados C., Mel'nikov S. Y., Grankin K. N., 2003, A&A, 409, 163
Paatz G., Camenzind M., 1996, A&A, 308, 77
Press W. H., Teukolsky S. A., Vetterling W. T., Flannery B. P., 2002, Numerical Recipes in C. Cambridge Univ. Press, Cambridge
Ramírez S. V. et al., 2004, AJ, 127, 2659
Rebull L. M. et al., 2002, AJ, 123, 1528
Rebull L. M., Stauffer J. R., Megeath T., Hora J., Hartmann L., 2005, BAAS, 37, 185.08
Rebull L. M., Stauffer J. R., Megeath S. T., Hora J. L., Hartmann L., 2006, ApJ, 646, 297
Rhode K. L., Herbst W., Mathieu R. D., 2001, AJ, 122, 3258
Roberts D. H., Lehar J., Dreher J. W., 1987, AJ, 93, 968
Samadi R., Fialho F., Costa J. E. S., Drummond R., Pinheiro Da Silva L., Baudin F., Boumier P., Jorda L., 2007, preprint (astro-ph/0703354)
Scargle J. D., 1982, ApJ, 263, 835
Shu F., Najita J., Ostriker E., Wilkin F., Ruden S., Lizano S., 1994, ApJ, 429, 781
Siess L., Forestini M., Dougados C., 1997, A&A, 324, 556
Siess L., Dufour E., Forestini M., 2000, A&A, 358, 593
Soderblom D. R., King J. R., Siess L., Jones B. F., Fischer D., 1999, AJ, 118, 1301
Stassun K. G., Mathieu R. D., Mazeh T., Vrba F. J., 1999, AJ, 117, 2941
Sung H., Bessell M. S., Chun M.-Y., Karimov R., Ibrahimov M., 2008, AJ, 135, 441
Sung H., Stauffer J. R., Bessell M. S., 2009, AJ, 138, 1116
Teixeira P. S. et al., 2006, ApJ, 636, L45
Zwintz K. et al., 2011, ApJ, 729, 20

This paper has been typeset from a TEX/LATEX file prepared by the author.